Catalysis Today 155 (2010) 116–122

Contents lists available at ScienceDirect

Catalysis Today

journal homepage: www.elsevier.com/locate/cattod

Effect of geometry on the thermal behavior of catalytic micro-combustors

Almerinda Di Benedetto [a,*], Valeria Di Sarli [a], Gennaro Russo [b]

[a] Istituto di Ricerche sulla Combustione - CNR, Via Diocleziano 328, 80124, Napoli, Italy
[b] Dipartimento di Ingegneria Chimica - Università degli Studi di Napoli Federico II, Piazzale Tecchio 80, 80125, Napoli, Italy

ARTICLE INFO

Article history:
Available online 14 March 2009

Keywords:
Catalytic micro-combustors
Geometry
CFD
3D simulations

ABSTRACT

When miniaturizing catalytic combustors from the macro- and meso-scale down to the micro-scale, some phenomena start playing a relevant role, such as heat losses toward the external environment and transverse diffusion with respect to the residence time. These phenomena may significantly affect the thermal behavior of catalytic micro-reactors.

In this work, three-dimensional computational fluid dynamics (CFD) simulations are run for studying the effect of the cross-sectional geometry on the ignition/extinction behavior of catalytic micro-combustors. Two different shapes of the cross-section are investigated, circular and square. Stability maps are built and compared for lean propane/air combustion at different inlet gas velocities.

Results demonstrate that, at low inlet velocities, the square cross-section channel is more resistant to extinction than the cylindrical channel. Furthermore, it is shown that, close to the ignition point, a strong coupling between fluid flow and superficial reaction rate is established. For both geometries, this coupling does not allow blowout to occur when increasing the inlet velocity up to the value limiting the laminar regime for the incoming flow.

1. Introduction

Micro-reactors are a promising technology for energy production, for example, in micro-electromechanical systems (MEMS). Due to the large energy density of hydrocarbons, micro-combustors (specific energy = 45 kJ/g) may substitute devices based on the use of traditional lithium battery systems (specific energy = 1.2 kJ/g) in portable electronics (i.e., laptop computers and cell phones) [1].

Scaling down from macro- to micro-reactors is not simple, since some phenomena negligible at the macro-scales become relevant at the micro-scales. First of all, miniaturizing macro-combustors leads to an increase of the surface area to volume ratio and then thermal and radical quenching may prevail [1–6]. Experimental and theoretical studies have shown that the ranges of operating conditions at which a flame may stabilize in micro-devices are very narrow [3–6].

In this context, it has been found that catalytic micro-combustors exhibit wider stability maps than homogenous micro-combustors [7,8]. The catalytic layer deposited on the reactor walls may allow sustaining chemical reactions at lower temperatures and in the presence of higher heat losses, thus reducing the impact of thermal quenching. However, in such reactors, thermal fluxes have to be properly managed in order to get stable operation.

Furthermore, the use of catalytic micro-combustors for MEMS requires high power density, which can be obtained by increasing the mass flow rate and thus gas velocity. On the other hand, to reach high conversions, the residence time should be relatively high which means that low gas velocities are needed. The reactor stability also has to face the application requirements.

Finally, at the small-scales, the transverse Péclet number (P), which compares the diffusion time to the convective time, may become of order unity, increasing the role of heat and mass diffusion with respect to the residence time.

All these issues have been addressed by building stability and operating maps of catalytic micro-combustors as functions of the main parameters, such as inlet gas velocity [7–12], fuel equivalence ratio [8–11], wall thermal conductivity [7,8,11], reactor length and gap size [8], and external heat transfer coefficient [7,8,10]. The operating regions have been found to be limited by extinction and blowout occurring at low and high Reynolds numbers, respectively.

In most of the theoretical studies dealing with catalytic micro-combustors, two-dimensional computational fluid dynamics (CFD) models have been adopted [7,9,11].

Two-dimensional models neglect the perimetral variations of velocity, temperature, species concentration, and heat and mass fluxes. At the small-scales, these variations may be relevant, given that the transverse Péclet number becomes of order unity.

* Corresponding author. Tel.: +39 0817622673; fax: +39 0817622915.
E-mail address: dibenede@irc.cnr.it (A. Di Benedetto).

0920-5861/$ – see front matter © 2009 Elsevier B.V. All rights reserved.
doi:10.1016/j.cattod.2009.01.048

Nomenclature

A	area of the micro-combustor cross-section
A_C	pre-exponential factor of the catalytic reaction rate
$C_{C_3H_8}$	propane mole concentration
C_p	specific heat of the gas mixture
$C_{p,i}$	specific heat of species i
d	characteristic length of the micro-combustor cross-section
d_w	wall thickness
D	fuel diffusion coefficient
$D_{i,mix}$	diffusion coefficient of species i
E_C	activation energy of the catalytic reaction rate
h	exterior convective heat transfer coefficient
h_i	specific enthalpy of species i
h_{mix}	specific enthalpy of the ideal-gas mixture
H	specific (sensible enthalpy + kinetic energy)
I	unity matrix
J_i	diffusion flux of species i
k	gas thermal conductivity
k_w	wall thermal conductivity
L	length of the micro-combustor
N_c	species number
p	pressure
P	transverse Péclet number
q	heat flux at the outer surface of the wall
r	radial coordinate
R	radius of the micro-combustor
R_C	catalytic reaction rate
Re	Reynolds number
$\Re$	universal gas constant
t_D	mass diffusion time
T	temperature
$T_{a,ext}$	external temperature
T_b	bulk gas temperature
T_{in}	inlet gas temperature
T_{ref}	reference temperature (taken to be 298 K)
T_w	wall temperature
$T_{w,a}$	perimeter averaged wall temperature
$T_{w,ext}$	temperature at the exterior wall surface
$T_{w,max}$	maximum wall temperature
V	gas velocity
V_{in}	inlet gas velocity
W_{mix}	mean molecular weight of the mixture
x	axial coordinate
y	propane mole fraction
y_b	bulk propane mole fraction
$y_{b,in}$	bulk propane mole fraction at the inlet section of the micro-combustor
$y_{b,out}$	bulk propane mole fraction at the outlet section of the micro-combustor
$y_{w,a}$	perimeter averaged wall propane mole fraction
Y	mass fraction
Y_i	mass fraction of species i

Greek symbols

μ	gas viscosity
o	inner perimeter of the micro-combustor
ρ	gas density
σ	stress tensor
ϕ	inlet fuel equivalence ratio
φ	tangential coordinate
ω_h	superficial heat production rate
$\omega_{y,i}$	superficial reaction rate of species i
Ω	inner cross-section of the micro-combustor

In a modeling work, Ramanathan et al. [13] have studied the ignition behavior of catalytic macro/meso-reactors by taking into account also the variations along the perimetral coordinate. They have simulated channels with circular, triangular, square, rectangular, sinusoidal and hexagonal cross-sections, showing that the shape of the cross-section may significantly affect ignition. More precisely, they have found that ignition is more favored in the presence of sharp corners rather than with smooth (circular) cross-section. For geometries having corners, the heat accumulated at the corners allows ignition to start near the corners and then to spread in the circumferential and axial directions.

In this work, a three-dimensional CFD model is adopted to study the effect of the cross-sectional geometry on the thermal behavior of catalytic micro-combustors. Two different shapes of the cross-section are investigated, circular and square. Stability maps are built and compared for lean propane/air combustion at different inlet gas velocities.

2. The model

A three-dimensional CFD model is developed to simulate the coupling between the fluid flow and the chemical processes at the gas/solid interface. The model solves the mass, momentum, species and energy conservation equations in the fluid along with the energy equation in the solid wall. Steady-state simulations are carried out.

The conservation equations in the fluid are listed below:

Continuity equation

$$\nabla \cdot (\rho V) = 0 \tag{1}$$

Momentum conservation equation

$$\nabla \cdot (\rho VV) = \nabla \cdot \sigma \tag{2}$$

with the stress tensor

$$\sigma = \left(-p + \frac{2}{3}\mu \nabla \cdot V\right) I + \mu \left[\nabla V + (\nabla V)^{\mathrm{T}}\right] \tag{3}$$

Species conservation equation

$$\nabla \cdot (\rho V Y_i) = \nabla \cdot (\rho J_i), \quad i = 1, 2, \ldots, N_c - 1 \tag{4}$$

where

$$J_i = D_{i,mix} \nabla Y_i \tag{5}$$

Energy conservation equation

$$\nabla \cdot (\rho VH) = \nabla \cdot (k \nabla T) + \nabla \cdot \left(\rho \sum_{i=1}^{N_c} J_i h_i\right) \tag{6}$$

with

$$H = h_{mix}(T, Y) + \tfrac{1}{2} V^2 \tag{7}$$

and

$$h_i(T) = \int_{T_{ref}}^{T} C_{p,i}(T) dT \tag{8}$$

The thermodynamic enthalpy of the ideal-gas mixture in Eq. (7) is expressed according to:

$$h_{mix}(T,Y) = \sum_{i=1}^{N_c} Y_i h_i(T) \tag{9}$$

The above equations are coupled to the ideal-gas equation:

$$\rho = \frac{pW_{mix}}{\Re T} \tag{10}$$

The energy equation in the solid wall reads:

$$k_w(\nabla^2 T_w) = 0 \tag{11}$$

where k_w is the solid thermal conductivity.

The catalytic reaction is assumed to be irreversible, first order in fuel concentration and zeroth order in oxygen concentration [12,14]. The reaction rate, referred to platinum as the catalyst, is calculated according to:

$$R_C\left[\frac{\text{kmol}_{C_3H_8}}{\text{m}^2\text{s}}\right] = A_C \cdot \exp\left(\frac{-E_C}{\Re T}\right) \cdot C_{C_3H_8} \tag{12}$$

The values of the pre-exponential factor and activation energy for Eq. (12) are equal to A_C = 2.4e + 5 m/s and $E_C/\Re = 10900\,1/\text{K}$.

At the inlet of the micro-combustor, a fixed flat velocity profile is assumed. For the energy and species equations, Danckwerts boundary conditions are used. At the exit, the static pressure is imposed as equal to the atmospheric pressure, and far-field conditions are specified for the remaining variables. At the fluid/wall interface, a no-slip boundary condition is assigned (the fluid has zero velocity relative to the boundary) along with the species balances (the mass flux of each species, ρJ_i, is equal to its rate of production/consumption, $\omega_{y,i}$):

$$\rho J_i = \omega_{y,i} \tag{13}$$

and the energy balance:

$$k\frac{\partial T}{\partial r} = k_w\frac{\partial T_w}{\partial r} + \omega_h \tag{14}$$

where ω_h is the superficial heat production rate.

Heat losses from the ends of the channel are not considered (insulated ends), while Newton's law of convection is used at the outer surface of the wall:

$$q = h(T_{w,ext} - T_{a,ext}) \tag{15}$$

where h is the exterior convective heat transfer coefficient, $T_{w,ext}$ is the temperature at the exterior wall surface, and $T_{a,ext}$ is the external temperature (taken to be 300 K).

The molecular viscosity is approximated through Sutherland's law for air viscosity. The fluid specific heat and thermal conductivity are calculated by a mass fraction weighted average of species properties.

The species specific heat is evaluated as a piecewise fifth-power polynomial function of temperature.

The full domains of the circular and square cross-section channels are considered, without using any conditions of symmetry.

The model equations are discretised using a finite volume formulation on a structured mesh built by means of the Gambit pre-processor of the Fluent package (version 6.3.26) [15].

Grid independent solutions are found by using a mesh with 190,400 and 230,400 cells for the circular and square cross-section channels, respectively.

The spatial discretisation of the model equations uses first-order schemes for all terms, except for the diffusion terms that are treated with a second-order central difference scheme.

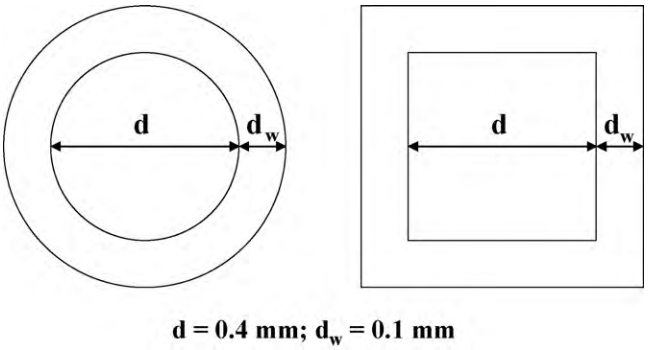

Fig. 1. Geometry of the channel cross-sections.

Table 1
Conditions adopted.

Parameter	Value
Solid thermal conductivity, k_w (W/(m K))	2
Inlet gas velocity, V_{in}	Varies
Inlet gas temperature, T_{in} (K)	300
Inlet fuel equivalence ratio, ϕ	0.8
Exterior convective heat transfer coefficient, h (W/(m^2 K))	20

Computations are performed by means of the segregated solver of the Fluent code [15] adopting the SIMPLE method to treat the pressure–velocity coupling. All residuals are always smaller than 1.0e–6.

3. Test cases

Fig. 1 shows the cross-sections, circular and square, of the two catalytic micro-combustors studied here. The values of the cross-section characteristic length (d) and the channel length (L) are equal to 0.4 and 10 mm, respectively. The wall thickness (d_w) is equal to 0.1 mm. In practical applications, the catalyst deposition tends to round the corners of the channel. Therefore, the two geometries of Fig. 1 can be seen as representative of extreme behaviors.

Table 1 summarizes the operating conditions adopted. The inlet velocity (V_{in}) is varied in a wide range (V_{in} = 0.3–100 m/s) corresponding to laminar conditions for the incoming flow.

From the computed solutions, the bulk gas temperature (T_b) and propane mole fraction (y_b) are calculated according to the following mass weighted average formulas:

$$T_b = \frac{\iint_\Omega \rho(\varphi,r)V(\varphi,r)C_p(\varphi,r)T(\varphi,r)dA}{\iint_\Omega \rho(\varphi,r)V(\varphi,r)C_p(\varphi,r)dA} \tag{16}$$

$$y_b = \frac{\iint_\Omega \rho(\varphi,r)V(\varphi,r)y(\varphi,r)dA}{\iint_\Omega \rho(\varphi,r)V(\varphi,r)dA} \tag{17}$$

where r and φ are the radial and tangential coordinates, respectively, and Ω the inner cross-section of the micro-combustor.

The perimeter averaged wall temperature ($T_{w,a}$) and propane mole fraction ($y_{w,a}$) can also be calculated:

$$T_{w,a} = \frac{1}{2\pi}\int_o T(\varphi)d\varphi \tag{18}$$

$$y_{w,a} = \frac{1}{2\pi}\int_o y(\varphi)d\varphi \tag{19}$$

where the symbol o indicates the inner perimeter of the micro-channel ($T_{w,a}$ and $y_{w,a}$ are calculated at the gas/solid interface).

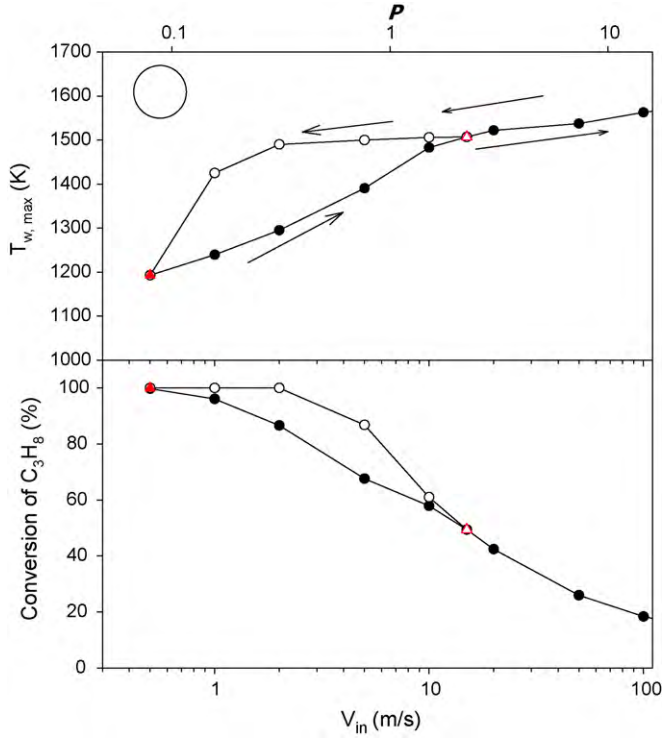

Fig. 2. Maximum wall temperature (top) and propane conversion (bottom) versus the inlet gas velocity (V_{in}); circular cross-section channel.

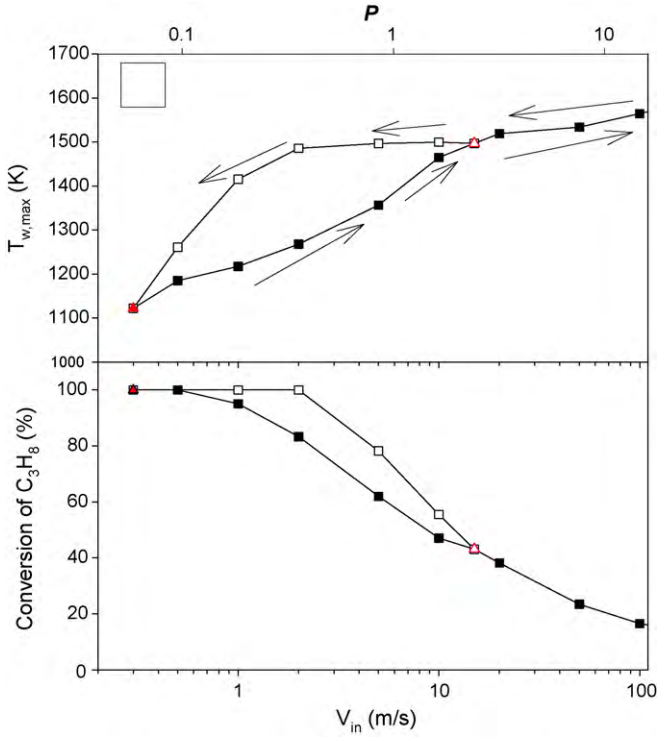

Fig. 3. Maximum wall temperature (top) and propane conversion (bottom) versus the inlet gas velocity (V_{in}); square cross-section channel.

4. Results and discussion

In the following, the stability maps of the two geometries investigated are first presented. Successively, the regimes identified on these maps are discussed.

4.1. Stability maps

In Figs. 2 and 3, the stability maps as obtained for the circular and square cross-section micro-combustors are shown in terms of the maximum wall temperature, $T_{w,max}$, versus the inlet velocity, V_{in}. The propane conversion as a function of V_{in} is also plotted in these figures. It is calculated as $100 \times (y_{b,in} - y_{b,out})/y_{b,in}$, with $y_{b,in}$ and $y_{b,out}$ bulk propane mole fraction at the inlet and outlet sections of the channel, respectively.

With both geometries, two bifurcation points are found at low and intermediate values of inlet velocity. At low inlet velocity, the bifurcation point corresponds to extinction. At intermediate inlet velocity, a hysteresis arises: steady-state multiplicity is found with two different solutions.

The hysteresis bifurcation point is found at $V_{in} \approx 15$ m/s for both micro-combustors. Extinction occurs at $V_{in} = 0.5$ m/s for the cylindrical channel and at $V_{in} = 0.3$ m/s for the square cross-section channel. In both cases, no blowout is found on increasing the inlet velocity up to the value limiting the laminar regime for the incoming flow (Re < 2000; $Vin = 100$ m/s).

In the stability maps of Figs. 2 and 3, the values of the transverse Péclet number (P) are also reported. This number gives a measure of the transverse diffusion time with respect to the convective time:

$$P = \frac{V_{in}R^2}{LD} \tag{20}$$

where R and L are the channel radius and length, respectively, and D is the fuel (i.e., propane) diffusion coefficient. It can be observed that the hysteresis bifurcation point arises at $P \approx 2$, when the diffusion and convective times become comparable.

The greater resistance to extinction found with the square cross-section micro-combustor can be related to the role of the corners in accumulating heat and generating local hot spots. For this geometry, Fig. 4 shows the temperature of the gas/solid interface as a function of the perimetral direction at three positions along the axial coordinate ($x = 0.1$, 0.25 and 0.5 mm, $V_{in} = 1$ m/s). It can be seen that the temperature profiles are not uniform and higher temperatures are attained at the corners.

In Fig. 4, the temperature field profile over the cross-section of the channel is also reported at an axial position corresponding to the ignition zone ($x = 0.1$ mm). The black line delineates the inner

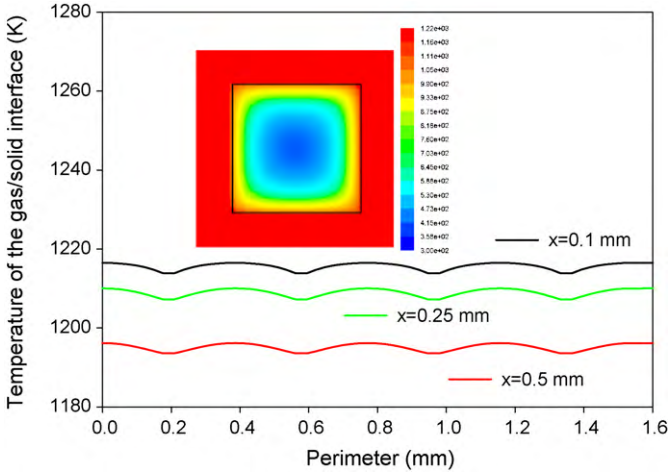

Fig. 4. Temperature of the gas/solid interface as a function of the perimetral direction at different axial positions along the square cross-section channel ($V_{in} = 1$ m/s, lower branch). The temperature field profile (K) over the cross-section of the channel is also reported ($x = 0.1$ mm) (the black line delineates the inner perimeter of the wall, separating the solid domain from the gas domain).

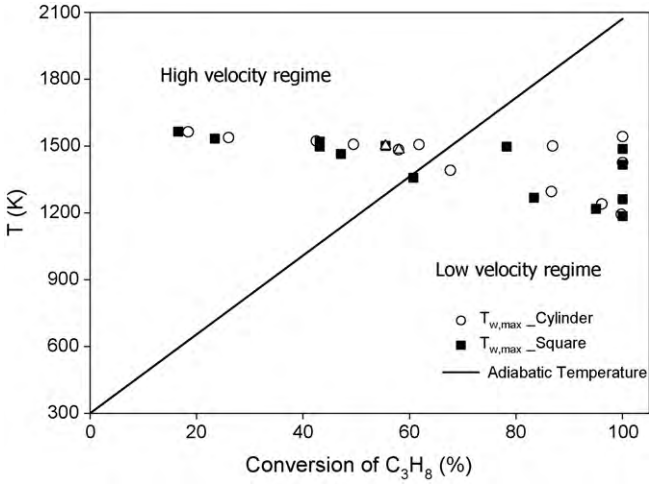

Fig. 5. Maximum wall temperature as a function of the propane conversion attained at the outlet for both circular and square cross-section channels. The adiabatic temperature corresponding to the outlet propane conversion is also plotted.

perimeter of the wall, separating the solid domain from the gas domain. The temperature difference across the solid thickness is estimated to be very small (less than 1 K).

The higher temperatures attained at the corners facilitate ignition, which occurs first at the corners and then spreads along the perimeter of the channel. This non-uniform ignition allows enlarging the range of inlet velocities at which the square cross-section micro-combustor is ignited. These results agree with the findings by Ramanathan et al. [13].

4.2. Regimes

From the above-presented maps, two main regimes may be distinguished for both the circular and square cross-section cases: the first regime (Regime I) corresponds to the low velocity range ($V_{in} < 15$ m/s), while the second regime (Regime II) corresponds to the high velocity range ($V_{in} > 15$ m/s). The hysteresis bifurcation point separates these two regimes.

Fig. 5 shows the maximum wall temperature of the circular and square cross-section micro-combustors as a function of the propane conversion attained at the outlet of the channels. For the low velocity regime, the results obtained by simulating both branches are reported.

By comparing the behaviors of Regime I and Regime II, a main difference can be found.

The variable discriminating between the two regimes is the temperature that would be reached at the channel outlet under adiabatic conditions. This temperature is here called *outlet adiabatic temperature* and is calculated, for each simulation, in correspondence to the outlet propane conversion. In the diagram of Fig. 5, the value of this temperature is also plotted.

It can be seen that the high velocity regime is characterized by low conversions (<50%) and maximum wall temperatures higher than the outlet adiabatic temperature. Conversely, the low velocity regime is characterized by high conversions (>50%) and maximum wall temperatures lower than the outlet adiabatic value.

4.2.1. Regime I (low velocity)

Within the low velocity regime ($V_{in} < 15$ m/s), there exists a steady-state multiplicity. Both branches exhibit high values of propane conversion (>50%) and maximum wall temperatures >1100 K.

In Fig. 6, the perimeter averaged wall temperature and the bulk gas temperature are plotted, together with the propane conversion, versus the axial position along the channel at $V_{in} = 1$ m/s, for both lower and upper branches of the square cross-section case. It can be seen that, while the propane conversions assume quite close values, the solid and gas temperatures in the lower branch are lower than in the upper branch.

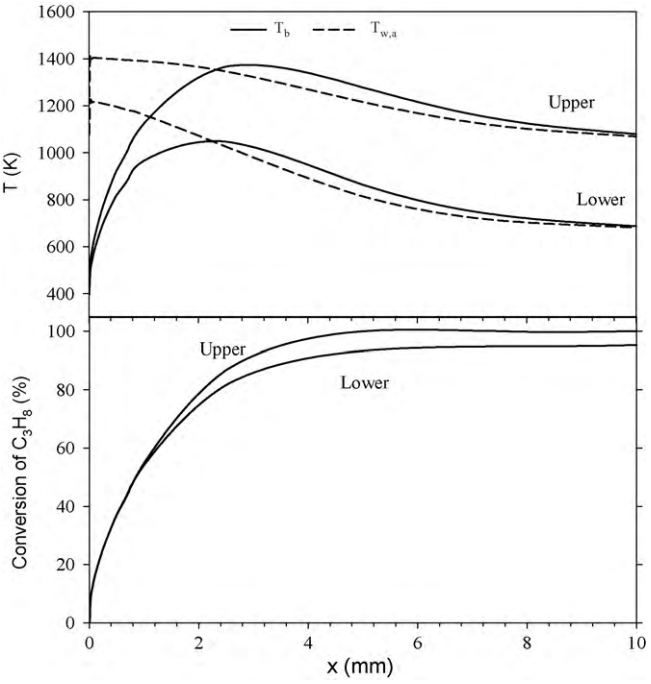

Fig. 6. Axial profiles of the perimeter averaged wall temperature and the bulk gas temperature (top) at $V_{in} = 1$ m/s in the upper and lower branches of the steady-state multiplicity (square cross-section channel). The propane conversion profiles are also reported (bottom).

The maximum differences between the conversions of the upper and lower branches are lower than 7%, while the maximum temperature differences are around 400 K. The small differences in conversion may be explained with the effect of the temperature variations on the diffusion coefficient (D) and thus on the diffusion time ($t_D \propto 1/T^{1.5}$), rather than with kinetic effects.

According to the temperature profile of Fig. 6, the micro-combustor may be divided into three main parts: a first part ($x < 2.4$ mm), where ignition takes place, that behaves as a heat source, a final part ($x > 4.6$ mm), whose behavior is similar to that of a heat sink (i.e., to that of a heat exchanger), and an intermediate part (2.4 mm $< x <$ 4.6 mm), where the channel behaves as "net" heat sink, given that the temperatures start decreasing, but there is still propane conversion and thus heat release. Starting from the second part of the micro-combustor, the bulk gas temperature overcomes the wall temperature. As a consequence, an inverse heat flux, from the gas to the solid wall, is established.

In previous papers [14,16], by means of a two-dimensional CFD model, we have shown that in the ignition zone, where superficial heat production occurs, the resulting gas expansion generates a perturbation to the fluid flow. The effect of this perturbation is similar to the entrance effect.

In Fig. 7 (top), the field profiles of the radial (left) and tangential (right) components of the gas velocity are shown as obtained over the square cross-section at an axial position close to the ignition point ($x = 0.1$ mm, $V_{in} = 1$ m/s). From these maps, it appears that the fluid starts to move driven by the heat production at ignition and that a recirculation of the fluid occurs.

The heat production at ignition leads to a three-dimensional perturbation of the flow field with the generation of a bulk

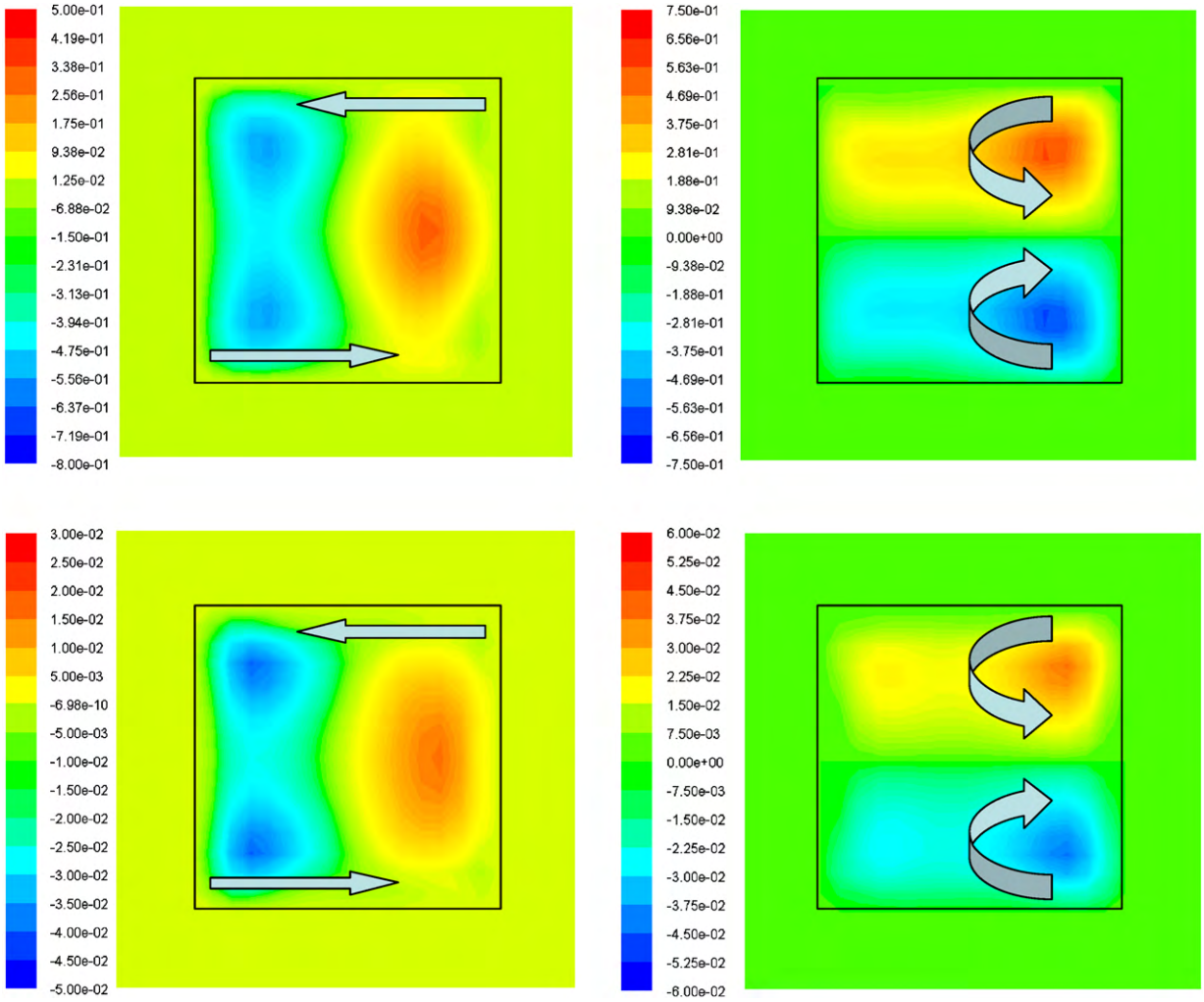

Fig. 7. Radial (left) and tangential (right) components of velocity, non-dimensionalised with the inlet velocity, at a fixed axial position along the square cross-section channel: V_{in} = 1 m/s and x = 0.1 mm (top); V_{in} = 50 m/s and x = 0.75 mm (bottom). The black lines delineate the inner perimeter of the walls, separating the solid domain from the gas domain.

rotational motion: at ignition, a *virtual obstacle* generates vortices that locally increase the gas residence time.

4.2.2. Regime II (high velocity)

In the high velocity regime ($V_{in} > 15$ m/s), the maximum wall temperature is high (1500–1600 K), while the propane conversion is relatively low (<50%). Furthermore, no blowout occurs (up to V_{in} = 100 m/s) and the maximum wall temperature does not decrease on increasing the inlet velocity (Figs. 2 and 3).

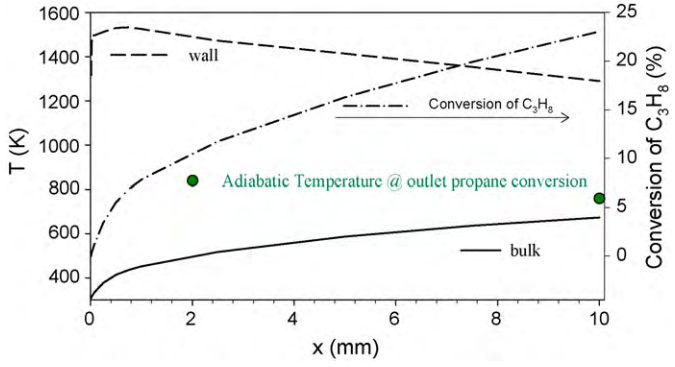

Fig. 8. Perimeter averaged wall temperature, bulk gas temperature, and propane conversion versus the axial position along the square cross-section channel (V_{in} = 50 m/s). The adiabatic temperature as calculated at the outlet propane conversion (≈25%) is also reported.

In Fig. 8, the perimeter averaged wall temperature and the bulk gas temperature are plotted versus the channel length at V_{in} = 50 m/s, for the square cross-section micro-combustor. In this figure, the axial profile of the propane conversion is also reported along with the value of the adiabatic temperature as calculated at the outlet propane conversion (≈25%).

From Fig. 8, it seems that the wall is unaffected by the heat exchange with the fluid phase. The wall temperature is almost constant along the entire channel length and higher than the adiabatic value corresponding to the outlet propane conversion (*under-exchanged conditions*). Also, the bulk gas temperature slightly increases along the channel length. However, it remains lower than the wall temperature. The high value of the wall temperature is the result of the coupling between the heat production due to catalytic reaction and the low heat exchange with the bulk gas phase. This heat exchange is limited by the low value of the residence time.

The absence of blowout may be addressed to the three-dimensional recirculation zones that arise at ignition. These vortices continuously feed propane to the wall increasing the mass transfer and then sustaining the catalytic reaction. The

generation of these recirculation zones is proven in Fig. 7 (bottom) where the radial (left) and tangential (right) components of velocity, non-dimensionalised with V_{in} = 50 m/s, are plotted over the cross-section of the combustor at x = 0.75 mm (i.e., close to the ignition position).

5. Summary and conclusions

Three-dimensional CFD simulations have been run for studying the role of the cross-sectional geometry on the thermal behavior of catalytic micro-combustors. Two different shapes of the cross-section have been investigated, circular and square. Stability maps have been built and compared for lean propane/air combustion at different inlet gas velocities.

The results obtained show that the square cross-section micro-reactor is more resistant to extinction than the cylindrical channel. This is due to the hot spots generated at the wall corners.

In both geometries, two main regimes have been identified by varying the inlet gas velocity:

(1) a low velocity regime ($V_{in} < 15$ m/s), with high propane conversions (>50%), at which a hysteresis occurs with two steady-state solutions;
(2) a high velocity regime ($V_{in} > 15$ m/s), with relatively low propane conversions (<50%), at which the wall temperature is much higher (order of 1600 K) than the bulk temperature (order of 800 K).

For both circular and square cross-section channels, it has been found that, in the high velocity regime, no blowout occurs when increasing the inlet velocity up to the value limiting the laminar regime for the incoming flow (V_{in} = 100 m/s). A possible explanation for this behavior is the presence of three-dimensional vortices that locally increase the gas residence time at the catalytic walls of the micro-combustors.

References

[1] A.C. Fernandez-Pello, Proc. Combust. Inst. 29 (2002) 883–899.
[2] P. Aghalayam, D.G. Vlachos, AIChE J. 44 (1998) 2025–2034.
[3] S. Raimondeau, D. Norton, D.G. Vlachos, R.I. Masel, Proc. Combust. Inst. 29 (2002) 901–907.
[4] D.G. Norton, D.G. Vlachos, Chem. Eng. Sci. 58 (2003) 4871–4882.
[5] D.G. Norton, D.G. Vlachos, Combust. Flame 138 (2004) 97–107.
[6] C.M. Spadaccini, A. Mehra, J. Lee, X. Zhang, S. Lukachko, I.A. Waitz, J. Eng. Gas Turbines Power 125 (2003) 709–719.
[7] S. Karagiannidis, J. Mantzaras, G. Jackson, K. Boulouchos, Proc. Combust. Inst. 31 (2007) 3309–3317.
[8] N.S. Kaisare, S.R. Deshmukh, D.G. Vlachos, Chem. Eng. Sci. 63 (2008) 1098–1116.
[9] K. Maruta, K. Takeda, J. Ahn, K. Borer, L. Sitzki, P.D. Ronney, O. Deutschmann, Proc. Combust. Inst. 29 (2002) 957–963.
[10] J. Hua, M. Wu, K. Kumar, Chem. Eng. Sci. 60 (2005) 3507–3515.
[11] D.G. Norton, E.D. Wetzel, D.G. Vlachos, Ind. Eng. Chem. Res. 45 (2006) 76–84.
[12] C.M. Spadaccini, J. Peck, I.A. Waitz, J. Eng. Gas Turbines Power 129 (2007) 49–60.
[13] K. Ramanathan, V. Balakotaiah, D.H. West, AIChE J. 50 (2004) 1493–1509.
[14] A. Di Benedetto, F. Donsì, F.S. Marra, G. Russo, Combust. Theor. Model. 9 (2005) 463–477.
[15] Fluent (version 6.3.26), Fluent Inc. www.fluent.com, 2008 (accessed 28.08.08).
[16] A. Di Benedetto, F. Donsì, F.S. Marra, G. Russo, AIChE J. 52 (2006) 911–923.